19

Measurement of Glucose Diffusion Coefficients in Human Tissues

Alexey N. Bashkatov, Elina A. Genina

Institute of Optics and Biophotonics, Saratov State University, Saratov, 410012, Russia

Valery V. Tuchin

Institute of Optics and Biophotonics, Saratov State University, Saratov, 410012, Russia,
Institute of Precise Mechanics and Control of RAS, Saratov 410028, Russia

In this chapter we have reviewed the main experimental methods, which are widely used for *in vitro* and *in vivo* measurements of glucose diffusion and permeability coefficients in human tissues. These methods are based on the spectroscopic and photoacoustic techniques, on the usage of radioactive labels for detecting matter flux, or on the measurements of temporal changes of the scattering properties of a tissue caused by refractive index matching including interferometric technique and optical coherence tomography. The methods provide reliable basis for measurement of glucose diffusion characteristics in tissues. The obtained results can be used in diagnostics and therapy of different diseases related to glucose impact.

Key words: glucose, optical clearing, diffusion coefficient, penetration, diabetes.

19.1 Introduction

Recent technological advancements in the photonics industry have led to a resurgence of interest in optical imaging technologies and real progress toward the development of noninvasive clinical functional imaging systems. Application of the optical methods for physiological-condition monitoring and cancer diagnostics, as well as for treatment, is a growing field due to simplicity, low cost, and low risk of these methods. In clinical dermatology, oncology, gastroenterology, and gynecology optical methods are widely used for vessels imaging, detection, localization, and treatment of subcutaneous malignant growths and photodynamic therapy. Frequently, the optical methods use dyes and drugs for cell sensitizing and enhancement of the local immune status of a tissue; therefore the development of noninvasive measurement techniques for monitoring of exogenous and endogenous (metabolic) agents in human tissues and determination of their diffusivity and permeability coefficients are very important for diagnosis and therapy of various human diseases.

Glucose is one of the most important carbohydrate nutrient sources and is fundamental to almost all biological processes. A significant role for physiological glucose monitoring is in the diagnosis and management of diabetes. Goal of diabetes management is maintenance of blood glucose levels via insulin injection, modified diet, exercise, or a combination of these. For successive diabetes therapy, regular measurement of blood glucose levels (up to five times per day) is required [1, 2]. Since current glucose sensing methods require invasive puncture of the skin to obtain a blood sample for analysis, efforts to develop noninvasive glucose detection techniques and implantable glucose sensors using optical methods have been important [3] (see also chapters 2–18).

A number of invasive and noninvasive techniques have been investigated for glucose monitoring, including use of implanted sensors, reverse iontophoresis, direct transmission through blood vessels, measurement of glucose in interstitial fluid in the dermis, light transmission through or light reflection from blood containing body parts (including the ear-lobe, the lip, the finger, and the forearm), and optical examination of the aqueous humor of the eye [1, 3–7]; however, unfortunately, the problem of glucose monitoring in final form is not solved yet.

Another important problem of application of optical methods in medicine deals with the transport of laser (light) beam through fibrous tissues such as skin dermis, eye sclera, *dura mater*, etc. [8, 9]. Due to high scattering of visible and NIR radiation at propagation within these tissues, there are essential limitations on spatial resolution and light penetration depth for optical diagnostic and therapeutic methods to be successfully applied. Control of the tissue optical properties is a very appropriate way for solution of the problem. The temporary selective clearing of the upper tissue layers is the key technique for structural and functional imaging, particularly for detecting local static or dynamic inhomogeneities hidden within a highly scattering medium [10]. Aqueous glucose solutions are widely used for the control of tissue scattering properties [8–21]. Increase of glucose content in tissue reduces re-

fractive index mismatch and, correspondingly, decreases the scattering coefficient. On the other hand, measurement of the scattering coefficient allows one to monitor the change of glucose concentration in the tissue and blood, which is very important for monitoring of diabetic patients.

However, in spite of numerous investigations related to delivery of drug and cosmetic substances into human tissues and to control of the tissue optical properties the problem of estimating diffusion coefficient of the drugs and various chemicals, including glucose, in tissues has not been studied in detail. The knowledge of the diffusion coefficients is very important for development of mathematical models describing interaction between tissues and drugs, and, in particular, for evaluation of the drug and metabolic agent delivery through tissue.

Many biophysical techniques for study of penetration of various chemicals through living tissue and for estimation of the diffusion coefficients have been developed over the last fifty years. The methods are based on the fluorescence measurements [22–25] (including fluorescence correlation spectroscopy [25]), on the spectroscopic [26–33], Raman [34] and photoacoustic techniques [35,36], on the usage of radioactive labels for detecting matter flux [37–49], on the technique of nuclear magnetic resonance [50, 51], or on the measurements of temporal changes of the scattering properties of a tissue caused by dynamic refractive index matching [8–10, 12–21, 52–54] including interferometric technique [52–54] and optical coherence tomography (OCT) [20, 21]. However, fluorescence techniques cannot be used for direct measurement of glucose diffusion coefficients, although these techniques are very appropriate to measure protein diffusivity in tissues, and since the proteins are widely used for glucose detection then the techniques are important for development of new and increased accuracy of existing methods of glucose detection and monitoring. The spectroscopic, Raman, and photoacoustic methods have great potential for measuring glucose diffusion coefficients in tissues because the methods provide excellent sensitivity to glucose detection and monitoring, and the methods based on usage of radioactive labels for detecting matter flux and on the measurements of temporal changes of the scattering properties of the tissue are widely used for measurements of glucose diffusion and permeability coefficients now.

The purpose of this chapter is to review methods for measurement of glucose diffusion and permeability coefficients in human tissues *in vitro* and *in vivo*.

19.2 Spectroscopic Methods

The ability to measure noninvasively concentration of various chemicals in tissues could provide a variety of benefits for pharmacological research and, ultimately, clinical applications. In the previous section we described the technique of fluorescence measurements, which can be used for measurement of chemicals concentration and diffusion coefficient in biological tissues. However, many of exogenous

and metabolic agents (in particular glucose) are not fluorescent, and therefore cannot be directly measured by the fluorescence techniques. Therefore, for the direct detection of these substances and estimation of their diffusivity the optical absorption measurements can be performed [5, 26–33].

The method is based on the time-dependent measurement of the tissue optical absorbance in the spectral range, which corresponds to absorption bands of the substance under study. The transport of low-molecular chemicals within tissue can be described in the framework of free diffusion model [12–23, 27–49]. It is assumed that the following approximations are valid for the transport process: 1) only concentration diffusion takes place; *i.e.*, the flux of the chemical into tissue at a certain point within the tissue sample is proportional to the chemical concentration at this point; 2) the diffusion coefficient is constant over the entire sample volume; 3) penetration of a chemical into a tissue sample does not change the drug concentration in the external volume; 4) in the course of diffusion the chemical does not interact with tissue components.

Geometrically, the tissue sample can be presented as an infinite plane-parallel slab with a finite thickness. In this case, the one-dimensional diffusion problem has been solved. The one-dimensional diffusion equation of a drug transport has the form

$$\frac{\partial C(x,t)}{\partial t} = D\frac{\partial^2 C(x,t)}{\partial x^2}, \tag{19.1}$$

where $C(x,t)$ is the chemical concentration, D is the diffusion coefficient, t is the time, and x is the spatial coordinate.

The key approach in characterization of transfer of a chemical agent is that a set of boundary conditions defines the concentration profiles. Depending on the analytical solution used, tissue type, and the experimental setup, three kinds of initial and boundary conditions are most commonly used for studies of agent transport in tissues. All, however, are based on concentration $C(x,t)$ as determined by Fick's second law [Eq. (19.1)].

The initial condition corresponds to the absence of an agent inside the tissue before the measurements, *i.e.*,

$$C(x,0) = 0, \tag{19.2}$$

for all inner points of the tissue sample.

In the case when a tissue is presented as a slab, the three kinds of boundary conditions are the following:

1) A tissue slab free of agent is immersed in solution with the agent concentration of C_0

$$C(0,t) = C_0 \quad \text{and} \quad C(l,t) = C_0, \tag{19.3}$$

where l is a tissue sample thickness. The solution of Eq. (19.1) with the initial [Eq. (19.2)] and the boundary [Eq. (19.3)] conditions has the form [12, 15, 16, 18, 55]:

$$C(x,t) = C_0\left(1 - \sum_{i=0}^{\infty} \frac{4}{\pi(2i+1)} \sin\left(\frac{(2i+1)\pi x}{l}\right) \exp\left(-\frac{(2i+1)^2 D\pi^2 t}{l^2}\right)\right). \tag{19.4}$$

The integral of Eq. (19.4) over x gives another physical quantity, average concentration (total solute entering the tissue) as:

$$C(t) = C_0\left(1 - \frac{8}{\pi^2}\sum_{i=0}^{\infty} \frac{1}{(2i+1)^2} \exp\left(-(2i+1)^2 t\,\pi^2 D \Big/ l^2\right)\right), \tag{19.5}$$

where $C(t)$ is the volume-averaged concentration of an agent within tissue sample.

2) A tissue slab free of agent, one side of the slab contacts a solution with the agent concentration of $C_0$and the other side is isolated from agent penetration

$$C(0,t) = C_0 \quad \text{and} \quad \frac{\partial C(l,t)}{\partial x} = 0. \tag{19.6}$$

The solution of Eq. (19.1) with the initial [Eq. (19.2)] and the boundary [Eq. (19.6)] conditions has the form [27]:

$$C(x,t) = C_0\left(1 - \sum_{i=0}^{\infty} \frac{4}{\pi(2i+1)} \sin\left(\frac{(2i+1)\pi x}{2l}\right) \exp\left(-\frac{(2i+1)^2 D\pi^2 t}{4l^2}\right)\right). \tag{19.7}$$

The volume-averaged concentration in this case can be expressed as:

$$C(t) = C_0\left(1 - \frac{8}{\pi^2}\sum_{i=0}^{\infty} \frac{1}{(2i+1)^2} \exp\left(-(2i+1)^2 t\,\frac{\pi^2}{4} D \Big/ l^2\right)\right). \tag{19.8}$$

3) A tissue slab free of agent, where one side contacts a solution with the agent concentration of C_0, and the other side is kept at zero concentration

$$C(0,t) = C_0 \quad \text{and} \quad C(l,t) = 0. \tag{19.9}$$

The solution of Eq. (19.1) with the initial [Eq. (19.2)] and the boundary [Eq. (19.9)] conditions has the form [28–30,56]:

$$C(x,t) = C_0\left(1 - \frac{x}{l} - \sum_{i=1}^{\infty} \frac{2}{\pi i} \sin\left(\frac{i\pi x}{l}\right) \exp\left(-\frac{i^2 D\pi^2 t}{l^2}\right)\right). \tag{19.10}$$

The average concentration can be expressed as:

$$C(t) = \frac{C_0}{2}\left(1 - \frac{8}{\pi^2}\sum_{i=0}^{\infty} \frac{1}{(2i+1)^2} \exp\left(-(2i+1)^2 t\,\pi^2 D \Big/ l^2\right)\right). \tag{19.11}$$

When penetrating agent is administered to tissue topically and the tissue is a semi-infinite medium, *i.e.*, $x \in [0;\infty)$, the boundary conditions have the from:

$$C(0,t) = C_0 \quad \text{and} \quad C(\infty,t) = 0. \tag{19.12}$$

Solution of Eq. (19.1) with the initial [Eq. (19.2)] and the boundary [Eq. (19.12)] conditions, in this case, has the form [57]:

$$C(x,t) = C_0 \left(1 - \operatorname{erf}\left(\frac{x}{2\sqrt{Dt}}\right)\right), \tag{19.13}$$

where $\operatorname{erf}(z) = \frac{2}{\sqrt{\pi}} \int_0^z \exp\left(-a^2\right) da$ is the error function.

Several methods and instrumentations based on absorbance measurements have been developed for estimation of agent diffusion coefficients. The methods using the attenuated total reflectance Fourier transform infrared (ATR-FTIR) spectroscopy [28–32], spatially-resolved reflectance spectroscopy [27, 33], and Raman spectroscopy [34] are available (see also chapters 5–8, 10, 12).

ATR-FTIR spectroscopy was used for measuring tissue absorption bands in the mid-infrared (mid-IR) spectral region and for study of diffusion of topically applied chemicals in the tissue. The mid-IR lies in the spectral range between 2.5 μm (4000 cm^{-1}) and 10 μm (1000 cm^{-1}). Bands in this spectral range correspond mainly to frequencies of fundamental molecular vibrations, which are characteristic of the specific chemical bonds. In contrast to the NIR spectral range contains combination and overtone bands that are broad and weak, bands in the mid-IR are sharp and have a higher absorption coefficient [4]. The ATR phenomenon occurs when radiation propagating through a medium with refractive index n_1 crosses an interface with another medium with lower refractive index n_2. If the incident beam crosses the interface at an angle, which is greater than the critical angle, defined as $\theta_c = \arcsin(n_2/n_1)$, the beam will penetrate slightly into the medium with lower refractive index as it is being totally reflected. If the medium with lower refractive index has absorption bands in the frequency range of the incident radiation, each penetration will result in an energy loss due to absorption. Energy losses due to scattering may also occur. These combined energy losses are amplified by successive reflections within the internal reflection element (IRE).

The ability of ATR spectroscopy to detect absorbance and scattering depends upon a number of factors, including the intensity, wavelength, and entry angle of the incident radiation, the absorption coefficient of the absorber, the degree of contact between the two media, the number of internal reflections, and the ratio of n_2 to n_1 [58]. According to ATR theory [59], the sensitivity of the technique is especially dependent upon energy coupling between the two media and the depth of beam penetration into the medium with the lower refractive index. Coupling can be increased by choosing IRE with refractive index close to, but greater than, the sample, while the depth of penetration can be increased by choosing an incident angle close to, but greater than, the critical angle.

For recording of the ATR-FTIR spectra Fourier transform infrared spectrometer equipped by ATR with ZnSe (refractive index is 2.42) or Ge (refractive index is 4.0) a crystal of rectangular shape can be used. Typically, the ATR-FTIR spectrum is obtained by the Fourier transform of 64 or 128 interferograms, where Happ-Genzel apodization is used [60]. Spectral analysis can be performed by band fitting based on a nonlinear least-squares search using Gaussian band intensity shapes of the form $I_i(\nu) = A_i \exp\left(-\left[(\nu - \omega_i)/W_i\right]^2\right)$, where I represents the infrared absorbance, ν is a current value of wave number, and ω, W, and A are frequency, width, and amplitude of the ith band, respectively.

When the spatially-resolved reflectance spectroscopy has been used for determination of agent diffusion coefficient in tissue, the approach suggested by Mourant et al. [33] can be applied. The method is based on the use of modified Lambert-Beer law and, in this case, tissue absorbance can be determined as

$$A = \mu_a \sigma \rho + G, \tag{19.14}$$

where μ_a is the absorption coefficient, ρ is the source-detector distance, σ is the differential factor of photon pathlength, taking into account the lengthening of photon trajectories due to multiple scattering, and G is the constant, defined by geometry of the experiment. To simplify calculations, $\rho\sigma$ can be replaced by parameter L, that is defined by both absorption and scattering tissue properties and source-detector distance. The source-detector distance is a parameter, which is defining sensitivity of parameter L to absorption or to scattering of the tissue. The large separation of the source and detector (from millimeters to centimeters) results in large distances of photon travel and therefore a strong sensitivity to absorption. On the other hand, because of strong absorption by hemoglobin bands and detector limitations, large-distance measurements are limited to a spectral range of about 600–950 nm, reducing the number of chemicals that can be monitored. Additionally, the spatial resolution is low due to the large tissue volume that is probed. For small source-detector distance (about a few hundreds microns), which is commensurable with photon free pathlength, parameter L is defined by tissue scattering properties only [33, 61, 62].

The penetration of an agent into a tissue increases the tissue absorbance in the spectral range corresponding to absorption bands of the agent substance. Thus, the tissue absorbance measured in different time intervals can be determined as

$$A(t,\lambda) = A(t=0,\lambda) + \Delta\mu_a(t,\lambda)L, \tag{19.15}$$

where t is the time interval, λ is the wavelength, $\Delta\mu_a(t,\lambda) = \varepsilon(\lambda)C(t)$ is the absorption coefficient of an agent within the tissue, $\varepsilon(\lambda)$ is the agent molar absorption coefficient, $C(t)$ is the agent concentration in the tissue, which can be described by one of a series of Eqs. (19.5), (19.8), (19.11) in dependence on drug delivery method and geometry of measurements, and $A(t=0,\lambda)$ is the tissue absorbance, measured at initial moment.

Thus, the equation

$$\Delta A(t,\lambda) = A(t,\lambda) - A(t=0,\lambda) = \Delta\mu_a(t,\lambda)L = \varepsilon(\lambda)C(t)L \tag{19.16}$$

can be used for calculation of the drug diffusion coefficient.

This set of equations represents the direct problem, *i.e.*, describes the temporal evaluation of the absorbance of a tissue sample dependent on agent concentration within the tissue. Based on measurement of the evolution of the tissue absorbance, the reconstruction of the drug diffusion coefficient in a tissue can be carried out. The inverse problem solution can be obtained by minimization of the target function

$$F(D) = \sum_{i=1}^{N_t} \left(A(D,t_i) - A^*(t_i)\right)^2, \tag{19.17}$$

where $A(D,t)$ and $A^*(t)$ are the calculated and experimental values of the time-dependent absorbance, respectively, and N_t is the number of time points obtained at registration of the temporal dynamics of the absorbance. To minimize the target function, the Levenberg-Marquardt nonlinear least-squares-fitting algorithm described in detail by Press et al. [63] can be used. Iteration procedure repeats until experimental and calculated data are matched.

Infrared and near-infrared absorption spectroscopy techniques became the basis for nondestructive chemometric analysis and therefore hold great potential for the development of noninvasive blood and tissue glucose measurement techniques. The optical absorption methods are based on the concentration-dependent absorption of specific wavelengths of light by glucose or other compounds of interest. In theory, a beam of radiation may be directed through a blood-containing portion of the body and the exiting light is analyzed to determine the content of glucose.

The mid-IR spectral bands of glucose and other carbohydrates have been assigned and are dominated by C–C, C–H, O–H, O–C–H, C–O–H, and C–C–H stretching and bending vibrations [4, 64, 65]. The 800–1200 cm^{-1} fingerprint region of the infrared spectrum of glucose has bands at 836, 911, 1011, 1047, 1076, and 1250 cm^{-1}, which have been assigned to C–H bending vibrations [4,64,66]. A 1026 cm^{-1} band corresponds to C–O–H bend vibration [4,66] and 1033 cm^{-1} band can be associated with the ν(C–O–H) vibration [66] or with the ν(C–O–C) vibration [67].

Despite the specificity offered by infrared absorption spectroscopy, its application to quantitative blood glucose measurement is limited. A strong background absorption by water and other components of blood and tissues severely limits the pathlength that may be used for transmission spectroscopy to roughly 100 μm or less. Further, the magnitude of the absorption peaks and the dynamic range required to record them make quantitation based on these sharp peaks difficult. Nonetheless, attempts have been made to quantify blood glucose using infrared absorption spectroscopy *in vitro* and *in vivo* [4, 6, 60, 68–71].

In contrast to the mid-IR the incident radiation in the NIR spectral range passes relatively easily through water and body tissues allowing moderate pathlengths to be used for measurements. Thus, a large amount of effort has been devoted to the

development of NIR spectroscopy (NIRs) techniques for noninvasive measurement of blood glucose [6] (see also chapters 5–8, 10).

In the NIR spectral range absorption bands of glucose have been connected with C–H, O–H, and N–H vibrations [3, 6, 64, 66]. The strongest bands are the broad O–H stretch at 3550 cm^{-1} (2817 nm) and the C–H stretch vibrations 2961 and 2947 cm^{-1}(3377 and 3393 nm). Possible combination bands are a second O–H overtone band at 939 nm (3νOH), and a second harmonic C–H overtone band at 1126 nm (3νCH). A first O–H overtone band can be assigned at 1408 nm (2νOH). The 1536 nm band can be assigned as an O–H and C–H combination band (νOH + νCH). The 1688 nm band is assigned as a C–H overtone band (2νCH). Other bands at wavelength longer than 2000 nm are possibly combinations of a C–H stretch and a CCH, OCH deformation at 2261 and 2326 nm (νCH + νCCH, OCH) [3, 72].

Though all methods of optical glucose sensing require use of a prediction model relating to optical measurements of glucose concentration, the broad overlapping peaks and a complicated nature of multi-component NIR spectra make single or dual wavelength models inadequate. NIR absorption bands may be significantly influenced by factors such as temperature, pH, and the degree of hydrogen bonding present; the unknown influence of background spectra further complicates the problem. For this reason, quantitative NIR spectroscopy has long relied on the development of very high-order multivariate prediction models and empirical calibration techniques. For this reason, high-order multivariate models, which incorporate analysis of entire spectra, must be used to extract NIR glucose information [6] (see also chapter 5).

For glucose detection in NIR spectral range, it can be useful to break the NIR region into the region from 700 to 1300 nm and the region from 2.0 to 2.5 μm. In the NIR region from 700 to 1300 nm optical detectors and sources are readily available and relatively easy to use, transmission through tissue is rather good, and transmissive fiber optics can be used to facilitate a probe design. However, glucose absorption bands are particularly weak in this region, and it may be difficult to acquire signals with substantial signal to noise ratio to allow robust measurement. Further in the NIR spectrum, a relative dip in the water absorbance spectrum opens a unique window in the 2.0 to 2.5 μm wavelength region. This window, saddled between two large water absorbance peaks, allows pathlengths or penetration depths of the order of millimeters and contains specific glucose peaks at 2.11, 2.27, and 2.33 μm [72]. Thus, this region may be very applicable for quantifiable glucose measurement using NIR spectroscopy.

In addition to NIRs, Raman spectroscopy can provide potentially rapid, precise, and accurate analysis of glucose concentration and biochemical composition (see chapter 12). Raman spectroscopy provides information about the inelastic scattering, which occurs when vibrational or rotational energy is exchanged with incident probe radiation. As with IR spectroscopic techniques, Raman spectra can be utilized to identify molecules such as glucose, because these spectra are characteristic of variations in the molecular polarizability and dipole moments. However, in contrast to infrared and NIRs, Raman spectroscopy has a spectral signature that is less influenced by water [4]. In addition, Raman spectral bands are considerably narrower

(typically 10–20 cm^{-1} in width [73]) than those produced in NIR spectral experiments. Raman also has the ability to permit the simultaneous estimation of multiple analytes, requires minimum sample preparation, and would allow for direct sample analysis [6]. Like infrared absorption spectra, Raman spectra exhibit highly specific bands, which are dependent on concentration. As a rule, for tissue Raman analysis the spectral region between 400 and 2000 cm^{-1}, commonly referred to as the "fingerprint region," was employed. Many different molecular vibrations lead to Raman scattering in this part of the spectrum. In many cases bands can be assigned to specific molecular vibrations and or molecular species, much aiding the interpretation of the spectra in terms of biochemical composition of the tissue. In this spectral range Raman spectrum of glucose contains bands with maxima at 420, 515, 830, 880, 1040, 1100, 1367, and 1460 cm^{-1} [6].

19.3 Photoacoustic Technique

Photoacoustic spectroscopy (PAS) can be used to acquire absorption spectra noninvasively from samples, including biological ones. The photoacoustic signal is obtained by probing the sample with a monochromatic radiation, which is modulated or pulsed. Absorption of probe radiation by the sample results in localized short-duration heating. Thermal expansion then gives rise to a pressure wave, which can be detected with a suitable transducer. An absorption spectrum for the sample can be obtained by recording the amplitude of generated pressure waves as a function of probe beam wavelength. The pulsed PA signal is related to the properties of turbid medium by the equation [4, 74]:

$$\mathrm{PA} = k\left(\beta \upsilon^n / C_p\right) E_0 \mu_{eff}, \tag{19.18}$$

where PA is the signal amplitude, k is the proportionality constant, E_0 is the incident pulse energy, β is the coefficient of volumetric thermal expansion, υ is the speed of sound in the medium, C_p is the specific heat capacity, n is a constant between one and two, depending on the particular experimental conditions, $\mu_{eff} = \sqrt{3\mu_a(\mu_a + \mu_s')}$, μ_a is the medium absorption coefficient, $\mu_s' = \mu_s(1-g)$ is the medium reduced or transport scattering coefficient, and μ_s and g are the medium scattering coefficient and anisotropy factor, respectively.

To generate PA signals efficiently, two conditions, referred to as thermal and stress confinements, must be met [75]. The time scale for heat dissipation of absorbed electromagnetic (EM) energy by thermal conduction can be approximated by $\tau_{th} \sim L_p^2/4D_T$, where L_p is a characteristic linear dimension of the tissue volume being heated (*i.e.*, the penetration depth of the EM wave or the size of the absorbing structure). Actually, heat diffusion depends on the geometry of the heated volume, and the estimation of τ_{th} may vary. Upon the absorption of a pulse with a temporal duration of τ_p, the thermal diffusion length during the pulse period can be estimated

by $\delta_T = 2\sqrt{D_T \tau_p}$, where D_T is the thermal diffusivity of the sample. The pulse width τ_p should be shorter than τ_{th} to generate PA waves efficiently, a condition that is commonly referred to as thermal confinement where heat diffusion is negligible during the excitation pulse. Similarly, the time for the stress to transit the heated region can be estimated by $\tau_{st} = L_p/c$, c is the speed of sound. The pulse width τ_p should be shorter than τ_{st}, a condition that is commonly referred to as stress confinement.

In the photoacoustic spectroscopy technique, the choice of a wavelength in a region of greater absorbance presents a great advantage to give a large magnitude of acoustic signal up to the limit of photoacoustic saturation. However, the optical penetration depth is reduced when the optical absorption increases, so the tissue thickness probed is more superficial. The compromise on the choice of the wavelength is thus obtained by a good signal to noise ratio and with a penetration as large as possible. Because high signal-to-noise measurements require reasonable penetration of the sample by the probe radiation, the NIR spectral region has been attractive for the measurements. The advantage of PAS is that the signal recorded is a direct result of absorption only, and scattering does not play a significant role in the acquired signal.

The basic equipment required to realize investigations based on the usage of photoacoustic spectroscopy includes a picosecond or nanosecond laser system, and a wide-band acoustic transducer, which can detect both high and low ultrasonic frequencies of acoustic pressure at once [76]. In photoacoustic systems for glucose detection pulsed laser sources with wavelength 355 nm [77], 780, 830, 1300, 1440, 1550 and 1680 nm [3], 1.064 μm [78], and 9.7 μm [74, 79] have been used. The outgoing ultrasound from the initial source reaches the tissue surface and then can be picked up by an ultrasound transducer. Since it serves only as an acoustic receiver, and the emission efficiency is of no importance, the detector for PA measurement can be specially designed to provide required sensitivity. The most often used ultrasound detectors are piezoelectric based; they have low thermal noise and high sensitivity and can provide a wide band from 20 kHz to 100 MHz [75, 76].

Although the previous works [74, 79] in the mid-infrared region demonstrated the potential of photoacoustics as a method of measuring glucose concentration, this wavelength region is not regarded as viable for human tissue studies because of the high water absorption that reduces penetration depths to microns. This penetration may not be sufficient to investigate blood constituents within human tissue, although interaction with interstitial fluid yields measurements, which correlate with blood glucose concentrations but with a time shift [74].

The spectral region that shows the most promise for absorption by the analytes within blood is within the "tissue window," around the 1–2 μm [3, 80]. Although measurements within this region are advantageous for tissue studies, due to reasonable penetration of the sample by the probe radiation, they coincide with a region of lower glucose absorption. Despite the fact, both *in vitro* and *in vivo* studies have been carried out in this spectral range to assess the feasibility of photoacoustic technique for noninvasive glucose detection [74, 79], and the investigation demonstrated applicability of PAS to measurement of glucose concentration (see also chapter 14). Greatest percentage of change in the photoacoustic response was observed in region

of the C–H second overtone at 1126 nm, with a further peak in the region of the second O–H overtone at 939 nm [74]. In addition, the generated pulsed PA time profile can be analyzed to detect the effect of glucose on tissue scattering, which is reduced by increasing glucose concentration [3, 4, 6, 8–21].

For study of glucose diffusion in human tissues the simple approach, which has been presented in Refs. [35] and [36], can be applied. In accordance with the approach the laser-induced heat/emission from the tissue served to increase the temperature, *i.e.*, pressure, which can be detected by a transducer. Integrating the transducer response over time the pressure signal $P(t)$, which is directly related to the amount of heat emitted by the tissue, can be obtained. The pulse is characterized through its maximum, both the amplitude ($P_{\max}$) and time delay ($t_{\max}$) of appearance with respect to the beginning of the pulse. The signal evolutions can be characterized by fitting the curves $P_{\max}$ versus t by an expression derived from a model of diffusion in a semi-infinite medium. The applied model has been shown to be in good agreement with diffusion pattern [81]. The mathematical expression used is [36]:

$$P_{\max}(t) = P_{\infty} + P_c \exp\left(t/\tau_D\right) \operatorname{erfc}\left(\sqrt{t/\tau_D}\right), \tag{19.19}$$

where P_c, P_{∞}, and τ_D are fitting parameters, and $\operatorname{erfc}(\sqrt{t/\tau_D}) = 1 - \operatorname{erf}\left(\sqrt{t/\tau_D}\right)$ is the complementary error function [see, Eq. (19.13)].

This model yields a characteristic time of diffusion τ_D, as well as a total diffusion amplitude $P_c + P_{\infty}$. While τ_D represents the time necessary for half of the glucose to penetrate into the depth of the tissue, the sum $P_c + P_{\infty}$ represents the global initial amount of the agent contributing to the signal. $P_{\max}$ denotes the main heat emission; $t_{\max}$ represents the time needed for the main heat emission in the tissue to diffuse towards its surface and to be detected. These two parameters, $P_{\max}$ and $t_{\max}$, serve to provide a macroscopic characterization of the diffusion process.

19.4 Use of Radioactive Labels for Detecting Matter Flux

Many investigations based on the usage of radioactive labels for detecting matter flux have been performed in last decades for studies of penetration of various chemicals through living tissue and for estimation of diffusion coefficient of the chemicals in the tissues [37–49]. This method has both some advantages and some disadvantages. The main advantage of this method is connected with the possibility of measurement of very small amount (concentration) of penetration agents and the main disadvantage is connected with a necessity of use of radioactive isotopes that can be dangerous, especially in case of *in vivo* measurements.

Typically, *in vitro* permeability experiments are performed using a side-by-side two-chamber diffusion cell and scintillation counter [37–42, 44–49]. In the two-chamber diffusion cell, the tissue sample is placed between the two chambers and

the radiolabeled penetration agent diffuses from a donor chamber through the tissue into an acceptor chamber, as a rule filled by PBS solution for preventing tissue drying. In case of *in vivo* measurements the radiolabeled agents can be intravenously injected and thereafter urine [44] or interstitial fluid [43] was collected to determine its radioactivity.

Analysis of agent diffusion through a membrane (that can be skin, mucous, sclera or other tissues) in this case can be performed on the basis of the first Fick's diffusion law. The law states that the steady state flux (J) of penetration agents per unit pathlength is proportional to the concentration gradient (ΔC) and the diffusion coefficient (D, cm^2/s) [37, 55, 82]:

$$J = -D\Delta C/l = P\Delta C. \tag{19.20}$$

Here $\Delta C = C_d - C_a$, C_d is the concentration of radiolabeled agent in the donor chamber and C_a is the concentration of the agent in the acceptor chamber ($\mathrm{g/cm}^3$), l is the membrane thickness (cm), and P is the permeability coefficient (cm/s). The negative sign indicates that the flux is in the direction of the lower concentration. On the other hand, the permeability coefficient can be defined as [37, 55, 82]:

$$P = J/(C_d - C_a) = KD/l, \tag{19.21}$$

where $K = k_{12}/k_{21}$ is the partition coefficient; k_{12} is the binding constant and k_{21} is the dissolution constant; J is the steady state flux of the radiolabeled agent measured in $\mathrm{g\cdot cm^{-2}\cdot s^{-1}}$. The partition coefficient can be estimated from [41]:

$$K = \frac{(\text{radioactivity in tissue})/(\text{weight of tissue})}{(\text{radioactivity in solution})/(\text{weight of solution})}. \tag{19.22}$$

In turn, the permeability coefficient deals with structural properties of the tissue (membrane) through the relation [38,42]:

$$P = \frac{\varepsilon D_0}{\tau l}, \tag{19.23}$$

where ε, τ, and l are the porosity, tortuosity of the diffusional pathway, and thickness of the membrane, respectively, D_0 is the diffusion coefficient of the penetration agents in the tissue (membrane) interstitial fluid, and the diffusion coefficient D_0 can be calculated using the Stokes-Einstein equation: $D_0 = kT/(6\pi\eta r_s)$, where k is Boltzmann's constant, T denotes the absolute temperature, η is the solvent viscosity, and r_s is hydrodynamic (Stokes) radius of the diffusing molecules.

In vitro the permeability coefficient can be calculated from the following equation [42, 45]:

$$P = \frac{V \cdot dC}{S \cdot C_0 \cdot dt}, \tag{19.24}$$

where dC/dt is the change in concentration per volume sample per unit time, and V is the volume of the acceptor chamber. Therefore, the quantity $V \cdot dC/dt$ is the

steady-state flux per unit time. S is the surface area of the membrane, and C_0 is the initial concentration of the diffusing agent. Note that the parameter (dC/dt) can be measured as the slope of linear region of the amount of permeant in the acceptor chamber versus time plot.

Using the technique, Horibe et al. [49] have found that permeability coefficient of mannitol through pigmented rabbit conjunctiva in the mucosal-to-serosal direction is $(27.70 \pm 4.33) \times 10^{-8}$ cm/s and in the serosal-to-mucosal direction is $(25.50 \pm 4.40) \times 10^{-8}$ cm/s. Grass and Sweetana [45] measured the permeability coefficients of L-glucose, D-glucose, and mannitol through rabbit jejunum as $(3.03 \pm 0.33) \times 10^{-6}$ cm/s, $(14.99 \pm 2.02) \times 10^{-6}$ cm/s, and $(3.59 \pm 0.22) \times 10^{-6}$ cm/s, respectively. Myung et al. [40] measure glucose diffusion flux across human, bovine, and porcine corneas and determine the diffusion coefficient in each type of cornea as $(3.0 \pm 0.2) \times 10^{-6}$ cm^2/s, $(1.6 \pm 0.1) \times 10^{-6}$ cm^2/s, and $(1.8 \pm 0.6) \times 10^{-6}$ cm^2/s, respectively. Ghanem et al. [46] have shown that permeability coefficient of full-thickness mouse skin for mannitol is 3×10^{-8} cm/s. Similar result has been obtained by Ackermann and Flynn [47] for glucose, urea, and glycerol with hairless mouse skin. Wang et al. [43] measure the permeability coefficient of D-glucose through rat jejunum and ileum as 7.54×10^{-5} cm/s and 2.45×10^{-5} cm/s, respectively. Larhed et al. [39] measure diffusion coefficient of mannitol in phosphate buffer and native pig intestinal mucus as 9.8×10^{-6} cm^2/s and 8.6×10^{-6} cm^2/s, respectively. Peck et al. [42] presented that diffusion coefficients of mannitol and sucrose in human epidermal membrane are $(9.03 \pm 0.3) \times 10^{-6}$ cm^2/s and $(6.98 \pm 0.2) \times 10^{-6}$ cm^2/s, respectively. It should be noted that mannitol has the same molecular weight as glucose and similar structure, and, thus, transport (diffusing) characteristics of the substance in tissues can be similar as for glucose. Khalil et al. [48] have found that diffusion coefficient of glucose in skin dermis is $(2.64 \pm 0.42) \times 10^{-6}$ cm^2/s, and the glucose diffusion coefficient in viable epidermis is $(0.075 \pm 0.050) \times 10^{-6}$ cm^2/s.

19.5 Light Scattering Measurements

19.5.1 Spectrophotometry

It is well known that the major source of scattering in tissues and cell structures is the refractive index mismatch between mitochondria and cytoplasm, extracellular media, and tissue structural components such as collagen and elastin fibers [83, 84]. The scattering properties of tissues (such as skin dermis, sclera, *dura mater*, etc.) are significantly changed due to action of osmotically active immersion liquids, in particular by glucose solutions [8–19]. Measurement of the scattering coefficient allows one to monitor the change of glucose concentration in the tissue and thus for measurement of glucose diffusion coefficient. The optical method for estimating the diffusion coefficient in a tissue has been suggested by Tuchin et al. [12]. This method is based on the measurement of temporal changes of the scattering properties

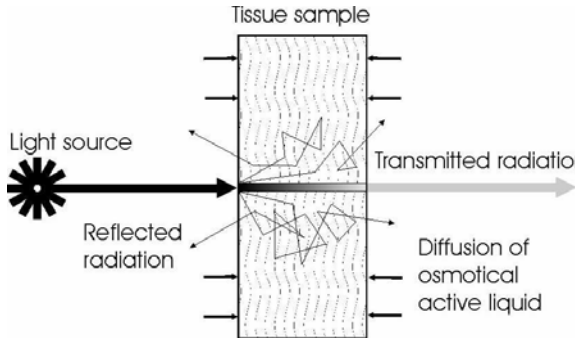

FIGURE 19.1: Schematic representation of osmotically active immersion liquid diffusion into the tissue sample and the geometry of light irradiation.

of a tissue caused by dynamics of refractive index matching. It can be used both for *in vitro* and *in vivo* measurements.

Experimentally, the simplest method for estimation of diffusion coefficients of osmotically active liquids in tissues is based on the time-dependent measurement of collimated transmittance of tissue samples placed in immersion liquid [8–10, 12–16, 18]. Schematic representation of the osmotically active immersion liquid diffusion into the tissue sample and the geometry of light irradiation are presented in Fig. 19.1. Since transport of immersion liquid (glucose solution) within the tissue can be described in the framework of the free diffusion model (see section 19.3), then Eqs. (19.4), (19.5), (19.7), (19.8), (19.10), and (19.11) can be used to describe the spatial and temporal evolution of glucose concentration within a tissue.

The time dependence of collimated optical transmittance of a tissue sample impregnated by an immersion solution is defined by Bouguer-Lambert law:

$$T_c(t) = (1 - R_s)^2 \exp\left(-\left(\mu_a + \mu_s(t)\right) l(t)\right), \tag{19.25}$$

where R_s is the specular reflectance and μ_a is the tissue absorption coefficient. Since glucose does not have strong absorption bands in the visible and near-infrared spectral regions, then the changes of collimated transmittance of a tissue sample can be described only by the behavior of the tissue scattering. $\mu_s(t)$ is the tissue time-dependent scattering coefficient and $l(t)$ is the time-dependent thickness of the tissue sample. The time dependence of the tissue thickness occurs due to osmotic activity of immersion agents, because it is well known that action of hypo-osmotic liquids on the tissue causes tissue cells swelling, and application of hyper-osmotic solutions causes shrinkage process [11]. Thus, the application of osmotically active liquids can be accompanied by tissue swelling or shrinkage, which should be taken into account.

Since aqueous glucose solutions have pH different from pH of the interstitial fluid of the native tissue, placing tissues sample into the solutions produces the swelling (shrinkage) process in dependence on pH of the solutions. The temporal dependence of the tissue sample volume can be described assuming that increasing tissue vol-

ume is the result of additional absorption of the osmotically active liquids [85] and decreasing tissue volume is the result of water loss from the tissue sample.

The temporal dependence of the swelling $H(t)$ and shrinkage $H_D(t)$ indices of the tissue sample can be calculated from weight measurements as [16]:

$$H(t) = \frac{M(t) - M(t=0)}{M(t=0)} = \frac{M_{\text{osm}}(t)}{M(t=0)} = \frac{V_{\text{osm}}(t) \times \rho_{\text{osm}}}{M(t=0)}, \tag{19.26}$$

$$H_D(t) = \frac{M(t=0) - M(t)}{M(t=0)} = \frac{M_{H_2O}(t)}{M(t=0)} = \frac{V_{H_2O}(t) \times \rho_{H_2O}}{M(t=0)}, \tag{19.27}$$

where $M(t)$ is mass of the tissue sample in the different moments in the swelling (shrinkage) process, $M_{\text{osm}}(t)$, $V_{\text{osm}}(t)$, and $\rho_{\text{osm}}(t)$ are mass, volume, and density of osmotically active liquid (glucose solution) absorbed by the tissue sample, respectively. Let $V(t)$ represent the volume of swelling (shrinkage) tissue, then

$$V(t) = V(t=0) \pm V_{\text{osm}}(t) = V(t=0) \pm H(t) M(t=0) / \rho_{\text{osm}}. \tag{19.28}$$

Here sign "plus" corresponds to swelling process and sign "minus" to shrinkage process.

The temporal dependence of swelling (shrinkage) index can be approximated by the following phenomenological expression [16]:

$$H(t) = A\left(1 - \exp\left(-t/\tau_s\right)\right). \tag{19.29}$$

Therefore, the temporal dependence of tissue volume during osmotically active liquid action [Eq. (19.28)] can be presented as

$$V(t) = V(t=0) \pm A\left(1 - \exp\left(-t/\tau_s\right)\right). \tag{19.30}$$

In this case A and τ_s are some phenomenological constants describing a swelling (shrinkage) process caused by glucose action. Volumetric changes of a tissue sample are mostly due to changes of its thickness $l(t)$, which can be expressed as

$$l(t) = l(t=0) \pm A^*\left(1 - \exp\left(-t/\tau_s\right)\right), \tag{19.31}$$

where $A^* = A/S$, and S is the tissue sample area. The constants A and τ_s can be obtained both from direct measurements of thickness or volume of tissue samples and from time-dependent weight measurements [16]. For example, for *dura mater* samples immersed in the mannitol solution, we have estimated parameter A as 0.21 and the parameter characterizing the swelling rate, *i.e.*, τ_s as 484 s. For *dura mater* samples immersed in glucose solution with concentration 0.2 g/ml, we have estimated the parameter A as 0.2 and τ_s as 528 s [16].

By changing volume of a tissue the swelling (shrinkage) produces the change of the volume fraction of the tissue scatterers, and thus the change of the scatterer packing factor and the numerical concentration (density or volume fraction), *i.e.*, number of the scattering particles per unit area (for long cylindrical particles, density

fraction) or number of the scattering particles per unit volume (for spherical particles, volume fraction). Taking into account Eq. (19.30), the temporal dependence of the volume fraction of the tissue scatterers is described as

$$\phi(t) = \frac{V_s}{V(t)} = \frac{\phi(t=0) \times V(t=0)}{V(t=0) \pm A(1-\exp(-t/\tau))}, \tag{19.32}$$

where V_s is the volume of the tissue sample scatterers.

The optical model of fibrous tissue can be presented as a slab with a thickness l containing scatterers (collagen fibrils) – thin dielectric cylinders with an average diameter of about 100 nm, which is considerably smaller than their lengths. These cylinders are located in planes, which are parallel to the sample surfaces, but within each plane their orientations are random. In addition to the small, so-called Rayleigh scatterers, the fibrils are arranged in individual bundles in a parallel fashion; moreover, within each bundle, the groups of fibers are separated from each other by large empty lacunae distributed randomly in space [86]. Collagen bundles show a wide range of widths (1 to 50 μm) and thicknesses (0.5 to 6 μm) [87, 88]. These ribbon-like structures are multiple cross-linked; their length can be a few millimeters. They cross each other in all directions but remain parallel to the tissue surface.

For noninteracting particles the time-dependent scattering coefficient $\mu_s(t)$ of a tissue is defined by the following equation

$$\mu_s(t) = N\sigma_s(t), \tag{19.33}$$

where N is the number of the scattering particles (fibrils) per unit area and $\sigma_s(t)$ is the time-dependent cross-section of scattering. The number of the scattering particles per unit area can be estimated as $N = \phi/(\pi a^2)$ [89], where ϕ is the volume fraction of the tissue scatterers and a is their radii. For typical fibrous tissues, such as sclera, *dura mater*, and skin dermis, ϕ is usually equal to 0.2-0.3 [86].

To take into account interparticle correlation effects which are important for tissues with densely packed scattering particles the scattering cross-section has to be corrected by the packing factor of the scattering particles, $(1-\phi)^{p+1}/(1-\phi(p-1))^{p-1}$ [84], where p is a packing dimension that describes the rate at which the empty space between scatterers diminishes as the total number density increases. For spherical particles the packing dimension is equal to 3, and the packing of sheet-like and rod-shaped particles is characterized by packing dimensions that approach 1 and 2, respectively. Thus, Eq. (19.33) has to be rewritten as

$$\mu_s(t) = \frac{\phi}{\pi a^2}\sigma_s(t)\frac{(1-\phi)^3}{1+\phi}. \tag{19.34}$$

In accordance with Mie theory [83], if incident light is nonpolarized, scattering properties of cylindrical particles (the collagen fibrils and fibers) can be described by following set of relations:

$$\sigma_s = 2aQ_s = 2a\frac{Q_{sI}+Q_{sII}}{2}, \tag{19.35}$$

where a is a radius of the cylinder and Q_s is an efficiency factor of the scattering.

$$Q_{sI} = \frac{2}{x}\left[|b_{0I}|^2 + 2\sum_{n=1}^{\infty}\left(|b_{nI}|^2 + |a_{nI}|^2\right)\right],$$

$$Q_{sII} = \frac{2}{x}\left[|a_{0II}|^2 + 2\sum_{n=1}^{\infty}\left(|a_{nII}|^2 + |b_{nII}|^2\right)\right],$$

$$a_{nI} = \frac{C_n V_n - B_n D_n}{W_n V_n + iD_n^2}, \quad b_{nI} = \frac{W_n B_n + iD_n C_n}{W_n V_n + iD_n^2}$$

$$a_{nII} = -\frac{A_n V_n - iC_n D_n}{W_n V_n + iD_n^2}, \quad b_{nII} = -i\frac{C_n W_n + A_n D_n}{W_n V_n + iD_n^2}$$

$$A_n = i\xi\left[\xi J_n'(\eta) J_n(\xi) - \eta J_n(\eta) J_n'(\xi)\right], \; D_n = n\cos\zeta\,\eta J_n(\eta) H_n^{(1)}(\xi)\left(\frac{\xi^2}{\eta^2} - 1\right)$$

$$B_n = \xi\left[m^2\xi J_n'(\eta) J_n(\xi) - \eta J_n(\eta) J_n'(\xi)\right], \; C_n = n\cos\zeta\,\eta J_n(\eta) J_n(\xi)\left(\frac{\xi^2}{\eta^2} - 1\right)$$

$$V_n = \xi\left[m^2\xi J_n'(\eta) H_n^{(1)}(\xi) - \eta J_n(\eta) H_n^{(1)'}(\xi)\right],$$

$$W_n = i\xi\left[\eta J_n(\eta) H_n^{(1)'}(\xi) - \xi J_n'(\eta) H_n^{(1)}(\xi)\right]$$

$$\xi = x\sin(\zeta), \quad \eta = x\sqrt{m^2 - \cos^2(\zeta)}.$$

Here ζ is the angle between direction of incident field and the axis of cylinder. If wave vector of the incident field is directed perpendicularly to the axis of cylinder ($\zeta = 90^\circ$), the coefficients a_{nI} and b_{nII} turn to zero, *i.e.*,

$$b_{nI}\left(\zeta = 90^0\right) = b_n = \frac{J_n(mx) J_n'(x) - mJ_n'(mx) J_n(x)}{J_n(mx) H_n^{(1)'}(x) - mJ_n'(mx) H_n^{(1)}(x)},$$

$$a_{nII}\left(\zeta = 90^0\right) = a_n = \frac{mJ_n(mx) J_n'(x) - J_n'(mx) J_n(x)}{mJ_n(mx) H_n^{(1)'}(x) - J_n'(mx) H_n^{(1)}(x)}.$$

Here $J_n(\rho)$ is the Bessel function of the 1-st kind of n-order, $H_n^{(1)}(\rho)$ is the Bessel function of the 3-rd kind of n-order, $m = n_s/n_I$ is the ratio of the refractive indices of

the particle (n_s) and surrounding medium (n_I), and $x = 2\pi a n_I/\lambda$ is the size parameter, where λ represent wavelength in the surrounding medium.

Asymmetry factor of light scattering g (average cosine of scattering angle) for the case of the infinite cylinder illuminated by nonpolarized light is defined by following relation [83]:

$$g = \langle \cos\theta \rangle = \frac{\int_0^{\pi} \frac{T_{11}}{T_{11\text{norm}}} \cos(\theta)\sin(\theta)\, d\theta}{\int_0^{\pi} \frac{T_{11}}{T_{11\text{norm}}} \sin(\theta)\, d\theta}, \tag{19.36}$$

$$T_{11} = \frac{|T_1|^2 + |T_2|^2}{2}, \quad T_{11\text{norm}} = \frac{|b_{0I} + 2b_{nI}\cos\theta|^2 + |a_{0II} + 2a_{nII}\cos\theta|^2}{2},$$

$$T_1 = b_{0I} + 2\sum_{n=1}^{\infty} b_{nI}\cos(n\theta), \quad T_2 = a_{0II} + 2\sum_{n=1}^{\infty} a_{nII}\cos(n\theta),$$

where T_1, T_2 are the components of the amplitude forward scattering matrix; T_{11} is the component of the scattering matrix.

For spherical particles (the nucleus and mitochondria in cells of epithelial tissue, *e.g.*, skin epidermis or mucous tissue) the scattering cross-section and anisotropy factor can be described as [83]:

$$\sigma_s = \left(\frac{\lambda^2}{2\pi n_I^2}\right) \sum_{n=1}^{\infty} (2n+1)\left(|a_n|^2 + |b_n|^2\right), \tag{19.37}$$

$$g = \frac{\lambda^2}{\pi n_I^2 \sigma_s}\left[\sum_{n=1}^{\infty} \frac{n(n+2)}{n+1} Re\left\{a_n a_{n+1}^* + b_n b_{n+1}^*\right\} + \sum_{n=1}^{\infty} \frac{2n+1}{n(n+1)} Re\left\{a_n b_n^*\right\}\right], \tag{19.38}$$

where a_n and b_n are the Mie coefficients, and a_n^* and b_n^* are their complex conjugates.

$$a_n = \frac{m\psi_n(mx)\,\psi_n'(x) - \psi_n(x)\,\psi_n'(mx)}{m\psi_n(mx)\,\xi_n'(x) - \xi_n(x)\,\psi_n'(mx)},$$

$$b_n = \frac{\psi_n(mx)\,\psi_n'(x) - m\psi_n(x)\,\psi_n'(mx)}{\psi_n(mx)\,\xi_n'(x) - m\xi_n(x)\,\psi_n'(mx)}.$$

Here, $\psi_n(\rho) = \rho J_n(\rho)$ and $\xi_n(\rho) = \rho H_n^{(1)}(\rho)$ are the Riccati-Bessel functions, $J_n(\rho)$ is the Bessel function of the first kind of the n-order, and $H_n^{(1)}(\rho)$ is the Bessel function of the 3-rd kind of the n-order.

The time dependence of the refractive index of the interstitial fluid can be derived using the law of Gladstone and Dale, which states that the resulting value represents an average of the refractive indices of the components related to their volume fractions [90]. Such dependence is defined as

$$n_I(t) = (1 - C(t))\, n_{\text{base}} + C(t)\, n_{\text{osm}}, \tag{19.39}$$

where n_{base} is the refractive index of the tissue interstitial fluid at the initial moment, and n_{osm} is the refractive index of the glucose solutions. Numerous values of refractive indices of interstitial fluid and other tissue components are presented in Refs. [10] and [86]. Wavelength dependence of aqueous glucose solution can be estimated as

$$n_{\text{osm}}(\lambda) = n_w(\lambda) + 0.1515C, \tag{19.40}$$

where $n_w(\lambda)$ is the wavelength dependence of water, and C is the glucose concentration, g/ml [91]. The wavelength dependence of water has been presented by Kohl et al. [92] as

$$n_w(\lambda) = 1.3199 + \frac{6.878 \times 10^3}{\lambda^2} - \frac{1.132 \times 10^9}{\lambda^4} + \frac{1.11 \times 10^{14}}{\lambda^6}. \tag{19.41}$$

As a first approximation, we can assume that during the interaction between the tissue and the immersion liquid (glucose solution) the size and refractive index of the scatterers does not change. This assumption is confirmed by the results presented by Huang and Meek [85]. In this case, all changes in the tissue scattering are connected with the changes of the refractive index of the interstitial fluid described by Eq. (19.39). The increase of the refractive index of the interstitial fluid decreases the relative refractive index of the scattering particles and, consequently, decreases the scattering coefficient.

This set of equations describing glucose concentration dependence on time represents the direct problem. The reconstruction of the diffusion coefficient of the glucose in tissue can be carried out on the basis of measurement of the temporal evolution of the collimated transmittance. The solution of the inverse problem can be obtained by minimization of the target function: $F(D) = \sum_{i=1}^{N_t} (T_c(D,t_i) - T_c^*(t_i))^2$, where $T_c(D,t)$ and $T_c^*(t)$ are the calculated and experimental values of the time-dependent collimated transmittance, respectively, and N_t is the number of time points obtained at registration of the temporal dynamics of the collimated transmittance.

The mannitol and glucose diffusion coefficients in the human sclera [18], *dura mater* [16], and rat skin [14] were estimated using the temporal dependence of the collimated transmittance and the method presented in this section. The diffusion coefficients are presented in Table 19.1. It is well known that diffusion coefficient increases with the increase of temperature of the solution. The temperature dependence was accounted for as $D(T_2) = D(T_1)\frac{T_2}{T_1}\frac{\eta(T_1)}{\eta(T_2)}$ [93]. Here $D(T)$ is diffusion coefficient at temperature T and $\eta(T)$ is viscosity of the solution. The values of the diffusion coefficients, corrected to the physiological temperature of 37°C, are also presented in Table 19.1. The differences between the diffusion coefficients of these substances in water and in tissue are connected with the structure and composition of

the tissue interstitial matter, since the scleral, *dura mater*, and skin interstitial fluid contains the proteins, proteoglycans, and glycoproteins.

TABLE 19.1: The experimentally measured diffusion coefficients of glucose and mannitol in living tissues [14,16,18]

Tissue	Diffusing solution	Diffusion coefficient at 20 °C, cm^2 /s	Diffusion coefficient at 37 °C, cm^2 /s
Human sclera	20%-aqueous glucose solution	$(0.57 \pm 0.09) \times 10^{-6}$[18]	$(0.91 \pm 0.09) \times 10^{-6}$
Human sclera	30%-aqueous glucose solution	$(1.47 \pm 0.36) \times 10^{-6}$[18]	$(2.34 \pm 0.36) \times 10^{-6}$
Human sclera	40%-aqueous glucose solution	$(1.52 \pm 0.05) \times 10^{-6}$[18]	$(2.42 \pm 0.05) \times 10^{-6}$
Human *dura mater*	20%-aqueous glucose solution	$(1.63 \pm 0.29) \times 10^{-6}$[16]	$(2.59 \pm 0.29) \times 10^{-6}$
Human *dura mater*	20%-aqueous mannitol solution	$(1.31 \pm 0.41) \times 10^{-6}$ [16]	$(2.08 \pm 0.41) \times 10^{-6}$
Rat skin	40%-aqueous glucose solution	$(1.101 \pm 0.16) \times 10^{-6}$ [14]	$(1.75 \pm 0/1) \times 10^{-6}$

These measurements have been performed using a commercially available multichannel spectrometer LESA-6med (BioSpec, Russia) in transmittance mode. The scheme of the experimental setup is shown in Fig. 19.2. As a light source a 250 W xenon arc lamp with filtering of the radiation in the spectral range from 400 to 800 nm was used. During the *in vitro* light transmittance measurements, the glass cuvette with the tissue sample was placed between two optical fibers with a core diameter of 400 μm and a numerical aperture of 0.2. One fiber transmitted the excitation radiation to the sample, and another fiber collected the transmitted radiation. The 0.5-mm diaphragm placed 100 mm apart from the tip of the receiving fiber was used to provide collimated transmittance measurements. Neutral filter was used to attenuate the incident radiation.

The measurements have been performed every 30 seconds during 15–20 min for different human sclera and *dura mater* tissue samples. The experiments with the rat skin samples have been performed every 1 min at the beginning and every 5 min afterwards during about 190 min. Experimental error does not exceed 5% in the spectral range from 500 to 800 nm and 10% in the spectral range from 400 to 500 nm. All experiments have been performed at room temperature about 20°C.

Figure 19.3 illustrates the dynamics of collimated transmittance of skin sample measured at different wavelength concurrently with administration of 40% glucose

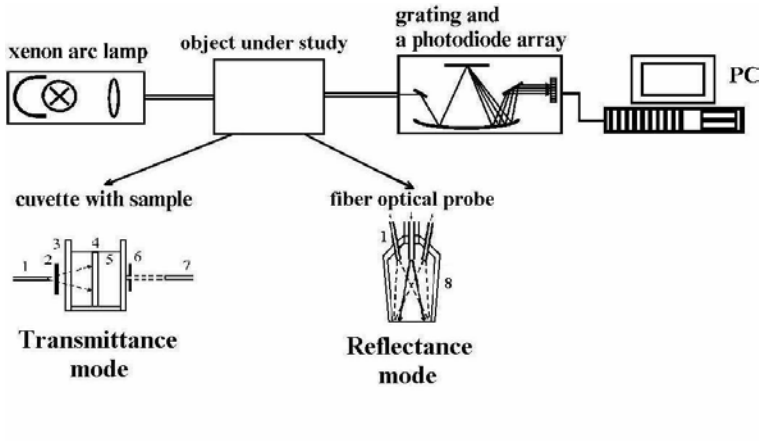

FIGURE 19.2: Experimental setup for measurements of collimated transmittance and reflectance spectra from tissue: 1 – optical irradiating fiber; 2 – neutral filters; 3 – cuvette; 4 – tissue sample; 5 – osmotically active immersion agent (the glucose and mannitol solutions); 6 – the 0.5 mm diaphragm; 7 – optical receiving fiber; 8 – aluminum holder.

solution [14]. It is easily seen that the untreated skin is a poorly transparent media for visible light. Glucose administration makes this tissue highly transparent; the 50-fold increase of the collimated transmittance is seen, and, as following from Fig. 19.3, the characteristic time response of skin optical clearing is about 1 hour. Using algorithm presented above, glucose diffusion coefficient in rat skin has been estimated as $(1.101 \pm 0.16) \times 10^{-6}$ cm^2/s.

For *in vivo* measurements [17,19] the experimental setup has been used in reflectance mode (see Fig. 19.2). The *in vivo* reflectance measurements were performed using an originally designed fiber optical probe with a system of optical fibers (designed by Yu.P. Sinichkin). The fibers were enclosed in a cone-shaped aluminum holder to provide a fixed distance between the fibers and tissue surface. Light from a stabilized light source (xenon arc lamp) was delivered to the tissue by means of the fiber fixed normally to the surface of tissue. The receiving fiber was displaced at an angle of 20 degrees to the sending fiber in such a way for the irradiated area to have a 5-mm diameter, and the area of light collection had a 10-mm diameter. Figure 19.4 presents the *in vivo* reflectance spectra of rabbit eye sclera measured at different time intervals after administration of 40%-glucose solution [13].

For calculation of tissue reflectance the Monte Carlo (MC) algorithm developed by Wang et al. [94] can be used. The stochastic numerical MC method is widely used to model optical radiation propagation in complex randomly inhomogeneous highly scattering and absorbing media such as biological tissues. Basic MC modeling of an individual photon packet's trajectory consists of the sequence of the elementary simulations [94]: photon pathlength generation, scattering and absorption events, reflection or/and refraction on the medium boundaries. The initial and final states

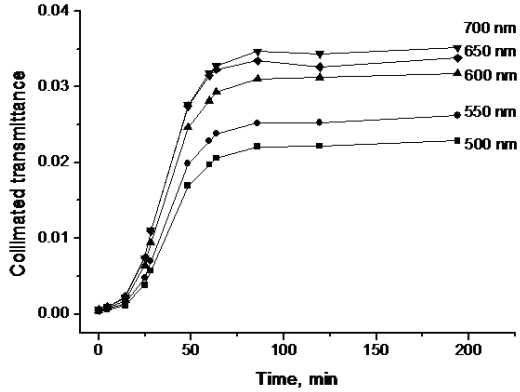

FIGURE 19.3: The time-dependent collimated transmittance of the rat skin samples (1 h after autopsy, hair were removed using tweezers) measured at different wavelength in a course of administration of 40%-aqueous solution in a bath [14].

of the photons are entirely determined by the source and detector geometry, *i.e.*, the incident light is assumed to be distributed on the area with diameter 5 mm, the photons' packets are launched normally to the tissue surface, and collected from the area with diameter 10 mm. At the site of scattering a new photon packet direction is determined according to the Henyey–Greenstein scattering phase function:

$$f_{\mathrm{HG}}(\theta) = \frac{1}{4\pi} \frac{1-g^2}{(1+g^2-2g\cos\theta)^{3/2}},$$

where θ is the polar scattering angle. The distribution over the azimuthal scattering angle was assumed as uniform. MC technique requires values of absorption and scattering coefficients, anisotropy factor, thickness and refractive index of tissues, and the required data and optical parameters can be calculated on the basis of Mie theory, previously measured or obtained from literature.

The calculation of glucose diffusion coefficient in tissue was carried out on the basis of measurement of the temporal evolution of the tissue optical reflectance. The solution of the inverse problem can be obtained by minimization of the target function: $F(D) = \sum_{i=1}^{N_t} \left(R(D,t_i) - R^*(t_i)\right)^2$, where $R(D,t)$ and $R^*(t)$ are the calculated and experimental values of the time-dependent reflectance, respectively, and N_t is the number of time points obtained at registration of the temporal dynamics of the reflectance. Using the approach the glucose diffusion coefficients in rabbit sclera *in vivo* has been measured as $(5.4 \pm 0.1) \times 10^{-7}$ cm^2/s [19].

Another approach for calculation of tissue reflectance connected with use of diffusion approximation of radiation transfer theory. According to the diffusion theory, the spatial dependence of the diffuse reflectance, $R(\rho)$, of continuous light remitted

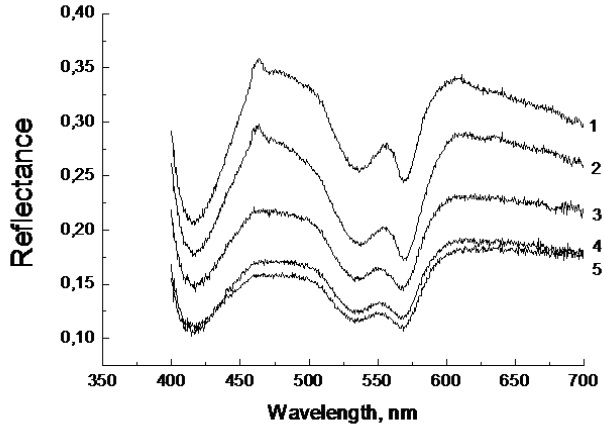

FIGURE 19.4: The *in vivo* time-dependent reflectance spectra of the rabbit eye sclera measured concurrently with administration of 40%-glucose solution: 1 — 1 min, 2 — 4 min, 3 — 21 min, 4 — 25 min, 5 — 30 min after drop of glucose solution onto the rabbit eye surface [13].

from a semi-infinite scattering medium at a separation of ρ from the source is [95]

$$R(\rho) = \frac{I_0}{4\pi\mu_t'}\left[\left(\mu_{\text{eff}} + \frac{1}{r_1}\right)\frac{e^{-\mu_{\text{eff}} r_1}}{r_1^2} + \left(\frac{4}{3}A + 1\right)\left(\mu_{\text{eff}} + \frac{1}{r_2}\right)\frac{e^{-\mu_{\text{eff}} r_2}}{r_2^2}\right], \quad (19.42)$$

where $r_1 = \sqrt{\left(1/\mu_t'\right)^2 + \rho^2}$, $r_2 = \sqrt{\left(\left(\frac{4}{3}A + 1\right)/\mu_t'\right)^2 + \rho^2}$, $\mu_t' = \mu_a + \mu_s'$, I_0 is the initial light source intensity, and A is an internal specular reflection parameter, depending only on the relative refractive index of the tissue and surrounding medium. For matching of this formula with geometry of the experiments the function $R(\rho)$ has been integrated over all area from which reflected radiance was collected. Using the approach the glucose diffusion coefficients in human skin *in vivo* has been measured as $(2.56 \pm 0.13) \times 10^{-6}$ cm^2/s [17].

19.5.2 OCT and interferometry

Optical coherence tomography is a new imaging technique, which provides images of tissues with resolution of about 10 μm or less at a depth of up to 1 mm depending on optical properties of tissue [96, 97]. It allows determination of refractive index and scattering coefficient values in layered structures in skin and other tissues. Since its introduction in 1991 several research groups actively developed the OCT technique for many diagnostic applications. In its most basic configuration, OCT system consists of a Michelson interferometer excited by a low temporal coherence

laser source, in-depth scanning system in the "reference" arm, an object under study in the "sample" arm, and registering photodiode at the output. Usually, the sample arm has additional scanning system that allows formation of cross-sectional two- and three-dimensional images of tissues. The interferometric signals in OCT system can be formed only when the optical path length in the sample arm matches that in the reference arm within the coherence length of the source. Therefore, the coherence length of the source and the group refractive index of tissues will determine the in-depth resolution of the OCT system [97].

Attenuation of light intensity for ballistic photons, I, in a medium with scattering and absorption is described by the Bouguer-Lambert law: $I = I_0 \exp(-2\mu_t z)$, where I_0 is the incident light intensity, $\mu_t = \mu_a + \mu_s$ is the attenuation coefficient for ballistic photons, μ_s and μ_a are the scattering and absorption coefficients, respectively, and z is the tissue probing depth. Since absorption in tissues is substantially less than scattering ($\mu_a \ll \mu_s$) in the NIR spectral range, the exponential attenuation of ballistic photons in tissue depends mainly on the scattering coefficient: $I = I_0 \exp(-2\mu_s z)$ [10]. Since the scattering coefficient of tissue depends on the bulk index of refraction mismatch, an increase in refractive index and the interstitial fluid and corresponding decrease in scattering can be detected as a change in the slope of fall-off of the depth-resolved OCT amplitude [10, 97–99].

The permeability coefficient of drug and solutions in tissues can be measured by OCT system and calculated using two methods, OCT signal slope (OCTSS) and OCT amplitude (OCTA) measurements [20] (see also chapter 20). With the OCTSS method, the average permeability coefficient of a specific region in the tissue can be calculated by analyzing the slope changes in the OCT signal caused by analyte diffusion. For this two-dimensional OCT images have to be averaged in the lateral (x-axial) direction into a single curve to obtain an OCT signal that represented the one-dimensional distribution of intensity in-depth. A region in the tissue, where the signal is linear and has minimal alterations, has to be selected, and its thickness (z_{region}) has to be measured. Diffusion of the agents in the chosen region has to be monitored, and time of diffusion has to be recorded (t_{region}). The average permeability coefficient ($\bar{P}$) can be calculated by dividing the measured thickness of the selected region by the time it took for the agent to diffuse through $\left(\bar{P} = \frac{z_{\text{region}}}{t_{\text{region}}}\right)$ [20].

The OCTA method can be used to calculate the permeability coefficient at specific depths in the tissues as $P(z) = z_i / t_{zi}$, where z_i is the depth at which measurements were performed (calculated from the front surface) and t_{zi} is the time of agent diffusion to the depth. The t_{zi} has to be calculated from the time agent was added to the tissue until agent-induced change in the OCT amplitude was commenced [20].

Using the methods, permeability coefficient of mannitol through rabbit cornea has been measured as $(8.99 \pm 1.43) \times 10^{-6}$ cm/s [20]. The permeability coefficients of mannitol and 20% glucose solution through rabbit sclera are measured as $(6.18 \pm 1.08) \times 10^{-6}$ and $(8.64 \pm 1.12) \times 10^{-6}$ cm/s, respectively [20]. The permeability coefficient of 20% glucose solution through pig's aorta tissue was found as $(1.43 \pm 0.24) \times 10^{-5}$ cm/s [21].

The interferometric methods [52–54] are also based on measurements of refractive

index variation. Holographic interferometry, electronic speckle pattern interferometry (ESPI), and digital holography have been successfully used to measure diffusion coefficients in liquids for binary systems and in membranes [54]. When applied to membranes, compared with traditional methods, ESPI offers the advantages of easily discriminating between a semi-permeable and a permeable membrane and the full control of experimental conditions gained by using a nonagitated cell [53].

For composite systems in which diffusion is one-dimensional, an interference pattern characterized by parallel fringes is obtained when an image taken during the diffusion process is subtracted from a reference image, usually obtained at time zero. In this case it is possible to obtain a concentration profile by using the position of the fringes. The diffusion coefficient can be calculated by fitting the concentration profile to a diffusion model like Fick's law.

Alternatively, an interference pattern characterized by two turning points is obtained by subtracting two images when fringes parallel to the direction of diffusion have been introduced during the diffusion coefficient [52]. When one concentration profile is subtracted from another, a typical concentration curve presenting a maximum and a minimum is obtained. The turning points of the interference pattern occur at a position where the maximum and the minimum of the concentration curve are located. The diffusion coefficient can be calculated by measuring the distance between the turning points. This second method offers the advantage of the faster calculation process, especially in the case when the diffusion problem can be solved analytically [54]. Using the method, Marucci et al. [54] measured the glucose diffusion coefficient in a model cellulose membrane and the diffusion coefficient is equal to $(1.6 \pm 0.15) \times 10^{-7}$ cm^2/s.

19.6 Conclusion

In this chapter we have reviewed the main experimental methods that are widely used for *in vitro* and *in vivo* measurements of glucose diffusion and permeability coefficients in human tissues. Importance of these investigations deals with glucose monitoring in the diagnosis and management of diabetes. Moreover, knowledge of the transport characteristics is very important for development of mathematical models describing interaction between tissues and drugs, and, in particular, for evaluation of the drug and metabolic agent delivery through the tissue.

These methods are based on the spectroscopic and photoacoustic techniques, on the usage of radioactive labels for detecting matter flux, or on the measurements of temporal changes of the scattering properties of a tissue caused by dynamic refractive index matching including interferometric technique and optical coherence tomography. As discussed in section 19.2, the absorbance spectroscopy and photoacoustics (section 19.3) can be used for measurement of glucose diffusion coefficients in the NIR and mid-infrared spectral ranges; the technique based on refractive index

matching (section 19.5) is of great importance for measurement of the glucose diffusion and permeability coefficients in the visible. Usage of radioactive labels for detecting matter flux (section 19.4) provides a powerful instrument for independent (reference) measurement of transport characteristics of glucose in tissues, because all spectral measurements depend on intrinsic tissue properties.

Indeed, in this chapter we reviewed only the main methods of measurement of diffusion characteristics of various chemicals in tissues but these methods provide reliable basis for measurement of glucose diffusion characteristics in the tissues, and the obtained results can be used in diagnostics and therapy of different diseases related to glucose impact.

Acknowledgments

This work has been supported in part by grants PG05-006-2 and REC-006 of U.S. Civilian Research and Development Foundation for the Independent States of the Former Soviet Union (CRDF) and the Russian Ministry of Science and Education, and grant of RFBR No. 06-02-16740-a. The authors thank Dr. S.V. Eremina (Department of English and Intercultural Communication of Saratov State University) for the help in manuscript translation to English.

References

[1] D.C. Klonoff, "Continuous glucose monitoring," *Diabetes Care*, vol. 28, 2005, pp. 1231-1239.

[2] D.B. Sacks, D.E. Bruns, D.E. Goldstein, et al., "Guidelines and recommendations for laboratory analysis in the diagnosis and management of diabetes mellitus," *Clin. Chem.*, vol. 48, 2002, pp. 436-472.

[3] O.S. Khalil, "Spectroscopic and clinical aspects of noninvasive glucose measurements," *Clin. Chem.*, vol. 45, 1999, pp. 165-177.

[4] O.S. Khalil, "Non-invasive glucose measurement technologies: an update from 1999 to the dawn of the new millennium," *Diab. Technol. Ther.*, vol. 6, 2004, pp. 660-697.

[5] R. Marbach, Th. Koschinsky, F.A. Gries, et al., "Noninvasive blood glucose assay by near-infrared diffuse reflectance spectroscopy of the human inner lip," *Appl. Spectrosc.*, vol. 47, 1993, pp. 875-881.

[6] R.J. McNichols and G.L. Coté, "Optical glucose sensing in biological fluids: an overview," *J. Biomed. Opt.*, vol. 5, 2000, pp. 5-16.

[7] J.C. Pickup, F. Hussain, N.D. Evans, et al., "In vivo glucose monitoring: the clinical reality and the promise," *Biosens. Bioelectr.*, vol. 20, 2005, pp. 1897-1902.

[8] V.V. Tuchin, "Optical clearing of tissues and blood using the immersion method," *J. Phys. D: Appl. Phys.*, vol. 38, 2005, pp. 2497-2518.

[9] V.V. Tuchin, "Optical immersion as a new tool for controlling the optical properties of tissues and blood," *Laser Phys.*, vol. 15, 2005, pp. 1109-1136.

[10] V.V. Tuchin, *Optical Clearing in Tissues and Blood*, SPIE Press, Bellingham, WA, vol. PM 154, 2005.

[11] H. Liu, B. Beauvoit, M. Kimura, et al., "Dependence of tissue optical properties on solute-induced changes in refractive index and osmolarity," *J. Biomed. Opt.*, vol. 1, 1996, pp. 200-211.

[12] V.V. Tuchin, I.L. Maksimova, D.A. Zimnyakov, et al., "Light propagation in tissues with controlled optical properties," *J. Biomed. Opt.*, vol. 2, 1997, pp. 401-417.

[13] A.N. Bashkatov, V.V. Tuchin, E.A. Genina, et al., "The human sclera dynamic spectra: in-vitro and in-vivo measurements," *Proc SPIE* 3591, 1999, pp. 311-319.

[14] A.N. Bashkatov, E.A. Genina, I.V. Korovina, et al., "*In vivo* and *in vitro* study of control of rat skin optical properties by action of 40%-glucose solution," *Proc SPIE* 4241, 2001, pp. 223-230.

[15] A.N. Bashkatov, E.A. Genina, and V.V. Tuchin, "Optical immersion as a tool for tissue scattering properties control," In *Perspectives in Engineering Optics*, ed. K. Singh and V.K. Rastogi, Anita Publications, New Delhi, India, 2002, pp. 313-334.

[16] A.N. Bashkatov, E.A. Genina, Yu.P. Sinichkin, et al., "Glucose and mannitol diffusion in human *dura mater*," *Biophys. J.*, vol. 85, 2003, pp. 3310-3318.

[17] V.V. Tuchin, A.N. Bashkatov, E.A. Genina, et al., "*In vivo* investigation of the immersion-liquid-induced human skin clearing dynamics," *Techn. Phys. Lett.*, vol. 27, 2001, pp. 489-490.

[18] A.N. Bashkatov, E.A. Genina, Yu.P. Sinichkin, et al., "Estimation of the glucose diffusion coefficient in human eye sclera," *Biophys.*, vol. 48, 2003, pp. 292-296.

[19] E.A. Genina, A.N. Bashkatov, Yu.P. Sinichkin, et al., "Optical clearing of the eye sclera *in vivo* caused by glucose," *Quant. Electr.*, vol. 36, 2006, pp. 1119-1124.

[20] M.G. Ghosn, V.V. Tuchin, and K.V. Larin, "Nondestructive quantification of analyte diffusion in cornea and sclera using optical coherence tomography," *Invest. Ophthal. Vis. Sci.*, vol. 48, 2007, pp. 2726-2733.

[21] .V. Larin, M.G. Ghosn, S.N. Ivers, et al., "Quantification of glucose diffusion in arterial tissues by using optical coherence tomography," *Laser Phys. Lett.*, vol. 4, 2007, pp. 312-317.

[22] M.E. Johnson, D.A. Berk, D. Blankschtein, et al., "Lateral diffusion of small compounds in human stratum corneum and model lipid bilayer systems," *Biophys. J.*, vol. 71, 1996, pp. 2656-2668.

[23] A. Partikian, B. Olveczky, R. Swaminathan, et al., "Rapid diffusion of green fluorescent protein in the mitochondrial matrix," *J. Cell Biology*, vol. 140, 1998, pp. 821-829.

[24] T.K.L. Meyvis, S.C. de Smedt, P. van Oostveldt, et al., "Fluorescence recovery after photobleaching: a versatile tool for mobility and interaction measurements in pharmaceutical research," *Pharm. Res.*, vol. 16, 1999, pp. 1153-1162.

[25] M. Weiss, H. Hashimoto, and T. Nilsson, "Anomalous protein diffusion in living cells as seen by fluorescence correlation spectroscopy," *Biophys. J.*, vol. 84, 2003, pp. 4043-4052.

[26] E.A. Genina, A.N. Bashkatov, Yu.P. Sinichkin, et al., *"In vitro* and *in vivo* study of dye diffusion into the human skin and hair follicles," *J. Biomed. Opt.*, vol. 7, 2002, pp. 471-477.

[27] E.A. Genina, A.N. Bashkatov, and V.V. Tuchin, "Methylene Blue diffusion in skin tissue," *Proc SPIE* 5486, 2004, pp. 315-323.

[28] F. Pirot, Y.N. Kalia, A.L. Stinchcomb, et al., "Characterization of the permeability barrier of human skin *in vivo,*" *Proc. Natl. Acad. Sci. USA*, vol. 94, 1997, pp. 1562-1567.

[29] A.L. Stinchcomb, F. Pirot, G.D. Touraille, et al., "Chemical uptake into human stratum corneum *in vivo* from volatile and non-volatile solvents," *Pharm. Res.*, vol. 16, 1999, pp. 1288-1293.

[30] J.-C. Tsai, C.-Y. Lin, H.-M. Sheu, et al., "Noninvasive characterization of regional variation in drug transport into human stratum corneum *in vivo*," *Pharm. Res.*, vol. 20, 2003, pp. 632-638.

[31] V. Buraphacheep, D.E. Wurster, and D.E. Wurster, "The use of Fourier transform infrared (FT-IR) spectroscopy to determine the diffusion coefficients of alcohols in polydimethylsiloxane," *Pharm. Res.*, vol. 11, 1994, pp. 561-565.

[32] T. Hatanaka, M. Shimoyama, K. Sugibayashi, et al., "Effect of vehicle on the skin permeability of drugs: polyethylene glycol 400-water and ethanol-water binary solvents," *J. Control. Release*, vol. 23, 1993, pp. 247-260.

[33] J.R. Mourant, T.M. Johnson, G. Los, et al., "Non-invasive measurement of chemotherapy drug concentrations in tissue: preliminary demonstrations of *in vivo* measurements," *Phys. Med. Biol.*, vol. 44, 1999, pp. 1397-1417.

[34] A.N. Yaroslavskaya, I.V. Yaroslavsky, C. Otto, et al., "Water exchange in human eye lens monitored by confocal Raman microspectroscopy," *Biophys.*, vol. 43, 1998, pp. 109-114.

[35] F. Lahjomri, N. Benamar, E. Chatri, et al., "Study of the diffusion of some emulsions in the human skin by pulsed photoacoustic spectroscopy," *Phys. Med. Biol.*, vol. 48, 2003, pp. 2729-2738.

[36] G. Puccetti, F. Lahjomri, and R.M. Leblanc, "Pulsed photoacoustic spectroscopy applied to the diffusion of sunscreen chromophores in human skin: the weakly absorbent regime," *J. Photochem. Photobiol. B*, vol. 39, 1997, pp. 110-120.

[37] I.H. Blank, J. Moloney, A.G. Emslie, et al., "The diffusion of water across the stratum corneum as a function of its water content," *J. Invest. Dermatol.*, vol. 82, 1984, pp. 188-194.

[38] T. Inamori, A.-H. Ghanem, W.I. Higuchi, et al., "Macromolecule transport in and effective pore size of ethanol pretreated human epidermal membrane," *Int. J. Pharm.*, vol. 105, 1994, pp. 113-123.

[39] A.W. Larhed, P. Artursson, and E. Bjork, "The influence of intestinal mucus components on the diffusion of drugs," *Pharm. Res.*, vol. 15, 1998, pp. 66-71.

[40] D. Myung, K. Derr, P. Huie, et al., "Glucose permeability of human, bovine, and porcine corneas in vitro," *Ophthal. Res.*, vol. 38, 2006, pp. 158-163.

[41] H. Okamoto, F. Yamashita, K. Saito, et al., "Analysis of drug penetration through the skin by the two-layer skin model," *Pharm. Res.*, vol. 6, 1989, pp. 931-937.

[42] K.D. Peck, A.-H. Ghanem, and W.I. Higuchi, "Hindered diffusion of polar molecules through and effective pore radii estimates of intact and ethanol treated human epidermal membrane," *Pharm. Res.*, vol. 11, 1994, pp. 1306-1314.

[43] Y. Wang, R. Aun, and F.L.S. Tse, "Absorption of D-glucose in the rat studied using *in situ* intestinal perfusion: a permeability-index approach," *Pharm. Res.*, vol. 14, 1997, pp. 1563-1567.

[44] F. Yamashita, H. Bando, Y. Koyama, et al., "*In vivo* and *in vitro* analysis of skin penetration enhancement based on a two-layer diffusion model with polar and nonpolar routes in the stratum corneum," *Pharm. Res.*, vol. 11, 1994, pp. 185-191.

[45] G.M. Grass and S.A. Sweetana, "*In vitro* measurement of gastrointestinal tissue permeability using a new diffusion cell," *Pharm. Res.*, vol. 5, 1988, pp. 372-376.

[46] A.-H. Ghanem, H. Mahmoud, W.I. Higuchi, et al., "The effects of ethanol on the transport lipophilic and polar permeants across hairless mouse skin: methods/validation of a novel approach," *Int. J. Pharm.*, vol. 78, 1992, pp. 137-156.

[47] C. Ackermann and G.L. Flynn, "Ether-water partitioning and permeability through nude mouse skin in vitro. I. Urea, thiourea, glycerol and glucose," *Int. J. Pharm.*, vol. 36, 1987, pp. 61-66.

[48] E. Khalil, K. Kretsos, and G.B. Kasting, "Glucose partition coefficient and diffusivity in the lower skin layers," *Pharm. Res.*, vol. 23, 2006, pp. 1227-1234.

[49] Y. Horibe, K.-I. Hosoya, K.-J. Kim, et al., "Polar solute transport across the pigmented rabbit conjunctiva: size dependence and the influence of 8-bromo cyclic adenosine monophosphate," *Pharm. Res.*, vol. 14, 1997, pp. 1246-1251.

[50] M.A. Fernandez-Seara, S.L. Wehrli, and F.W. Wehrli, "Diffusion of exchangeable water in cortical bone studied by nuclear magnetic resonance," *Biophys. J.*, vol. 82, 2002, pp. 522-529.

[51] D. Wang, U. Kreutzer, Y. Chung, et al., "Myoglobin and hemoglobin rotational diffusion in the cell," *Biophys. J.*, vol. 73, 1997, pp. 2764-2770.

[52] N. Bochner and J. Pipman, "A simple method of determining diffusion constants by holographic interferometry," *J. Phys. D: Appl. Phys.*, vol. 9, 1976, pp. 1825-1830.

[53] M. Marucci, G. Ragnarsson, and A. Axelsson, "Electronic speckle pattern interferometry: a novel non-invasive tool for studying drug transport rate and drug permeability through free films," *J. Control. Release*, vol. 114, 2006, pp. 369-380.

[54] M. Marucci, S.-G. Pettersson, G. Ragnarsson, et al., "Determination of a diffusion coefficient in a membrane by electronic speckle pattern interferometry: a new method and a temperature sensitivity study," *J. Phys. D: Appl. Phys.*, vol. 40, 2007, pp. 2870-2880.

[55] A. Kotyk and K. Janacek, *Membrane Transport: An Interdisciplinary Approach*, Plenum Press, New York, 1977.

[56] A.C. Watkinson and K.R. Brain, "Basic mathematical principles in skin permeation," *J. Toxicology (Cutaneous and ocular toxicology)*, vol. 21, 2002, pp. 371-402.

[57] G.M. Prusakov, *Mathematical Models and Methods in PC Calculations*, Nauka, Moscow, 1993.

[58] R.O. Potts, D.B. Guzek, R.R. Harris, et al., "A noninvasive, in vivo technique to quantitatively measure water concentration of the stratum corneum using attenuated total-reflectance infrared spectroscopy," *Arch. Dermatol. Res.*, vol. 277, 1985, pp. 489-495.

[59] N.J. Harrick, *Internal Reflection Spectroscopy*, Harrick Scientific Corporation, Ossining, NY, 1979.

[60] G.W. Lucassen, P.J. Caspers, and G.J. Puppels, "Infrared and Raman spectroscopy of human skin in vivo," In *Handbook of Optical Biomedical Diagnostics*, ed. V.V. Tuchin, SPIE Press, Bellingham, WA, 2002, pp. 787-823.

[61] J.R. Mourant, I.J. Bigio, D.A. Jack, et al., "Measuring absorption coefficients in small volumes of highly scattering media: source-detector separations for which path lengths do not depend on scattering properties," *Appl. Opt.*, vol. 36, 1997, pp. 5655-5661.

[62] F. Bevilacqua and C. Depeursinge, "Monte Carlo study of diffuse reflectance at source-detector separations close to one transport mean free path," *J. Opt. Soc. Am. A*, vol. 16, 1999, pp. 2935-2945.

[63] W.H. Press, S.A. Tuekolsky, W.T. Vettering, et al., *Numerical Recipes in C: the Art of Scientific Computing*, Cambridge University Press, Cambridge, 1992.

[64] P.D. Vasko, J. Blackwell, and J.L. Koenig, "Infrared and Raman spectroscopy of carbohydrates. I: Identification of O-H and C-H vibrational modes for D-glucose, malose, cellobiose, and dextran by deuterium substitution methods," *Carbohydr. Res.*, vol. 19, 1971, pp. 297-310.

[65] D.K. Buslov, N.A. Nikonenko, N.I. Sushko, et al., "Analysis of the results of α-D-glucose Fourier transform infrared spectrum de-convolution: comparison with experimental and theoretical data," *Spectrochim. Acta*, vol. 55, 1999, pp. 229-238.

[66] P.D. Vasko, J Blackwell, and J.L. Koenig, "Infrared and Raman spectroscopy of carbohydrates. II: Normal coordinate analysis of α-D- glucose," *Carbohydr. Res.*, vol. 23, 1972, pp. 407-417.

[67] C. Petibois, V. Rigalleau, A.-M. Melin, et al., "Determination of glucose in dried serum samples by Fourier-transform infrared spectroscopy," *Clin. Chem.*, vol. 45, 1999, pp. 1530-1535.

[68] S. Hahn and G. Yoon, "Identification of pure component spectra by independent component analysis in glucose prediction based on mid-infrared spectroscopy," *Appl. Opt.*, vol. 45, 2006, pp. 8374-8380.

[69] Y.J. Kim, S. Hahn, and G. Yoon, "Determination of glucose in whole blood samples by mid-infrared spectroscopy," *Appl. Opt.*, vol. 42, 2003, pp. 745-749.

[70] W.B. Martin, S. Mirov, and R. Venugopalan, "Using two discrete frequencies within the middle infrared to quantitatively determine glucose in serum," *J. Biomed. Opt.*, vol. 7, 2002, pp. 613-617.

[71] Y.C. Shen, A.G. Davies, E.H. Linfield, et al., "The use of Fourier-transform infrared spectroscopy for the quantitative determination of glucose concentration in whole blood," *Phys. Med. Biol.*, vol. 48, 2003, pp. 2023-2032.

[72] F.M. Ham, I.N. Kostanic, G.M. Cohen, et al., "Determination of glucose concentrations in an aqueous matrix from NIR spectra using optimal time-domain filtering and partial least-squares regression," *IEEE Trans. Biomed. Eng.*, vol. 44, 1997, pp. 475-485.

[73] E.B. Hanlon, R. Manoharan, T.W. Koo, et al., "Prospects for *in vivo* Raman spectroscopy," *Phys. Med. Biol.*, vol. 45, 2000, R1-R59.

[74] H.A. MacKenzie, Ashton H.S., S. Spiers, et al., "Advances in photoacoustic noninvasive glucose testing," *Clin. Chem.*, vol. 45, 1999, pp. 1587-1595.

[75] M. Xu and L.V. Wang, "Photoacoustic imaging in biomedicine," *Rev. Sci. Instr.*, vol. 77, 2006, 041101.

[76] A.A. Oraevsky and A.A. Karabutov, "Optoacoustic tomography," In *Biomedical Photonics Handbook*, ed. T. Vo-Dinh, Chap. 34, CRC Press, Boca Raton, FL, 2003.

[77] A.A. Bednov, A.K. Karabutov, E.V. Savateeva, et al., "Monitoring glucose in vivo by measuring laser-induced acoustic profiles," *Proc SPIE* 3916, 2000, pp. 9-18.

[78] K.M. Quan, G.B. Christison, H.A. MacKinzie, et al., "Glucose determination by a pulsed photoacoustic technique: an experimental study using a gelatin-based tissue phantom," *Phys. Med. Biol.*, vol. 38, 1993, pp. 1911-1922.

[79] G.B. Christison and H.A. MacKenzie, "Laser photoacoustic determination of physiological glucose concentrations in human whole blood," *Med. Biol. Eng. Comp.*, vol. 31, 1993, pp. 284-290.

[80] J.-L. Boulnois, "Photophysical processes in recent medical laser developments: a review," *Lasers Med. Sci.*, vol. 1, 1986, pp. 47-66.

[81] R.E. Imhof, C.J. Whitters, and D.J.S. Birch, "Time-domain opto-thermal spectro-radiometry," In *Photoacoustic and Photothermal Phenomena II*, J.C. Murphy, J.W. Maclachlan-Spicer, L. Aamodt et al. (eds.), Springer, Berlin, Heidelberg, 1990.

[82] H. Schaefer and T.E. Redelmeier, *Skin Barier: Principles of Percutaneous Absorption*, Karger, Basel et al., 1996.

[83] C.F. Bohren and D.R. Huffman, *Absorption and Scattering of Light by Small Particles*, Wiley, New York, 1983.

[84] J.M. Schmitt and G. Kumar, "Optical scattering properties of soft tissue: a discrete particle model," *Appl. Opt.*, vol. 37, 1998, pp. 2788-2797.

[85] Y. Huang and K.M. Meek, "Swelling studies on the cornea and sclera: the effects of pH and ionic strength," *Biophys. J.*, vol. 77, 1999, pp. 1655-1665.

[86] V.V. Tuchin, *Tissue Optics: Light Scattering Methods and Instruments for Medical Diagnosis*, vol. PM 166, SPIE Press, Bellingham, WA, 2007.

[87] I.S. Saidi, S.L. Jacques, and F.K. Tittel, "Mie and Rayleigh modeling of visible-light scattering in neonatal skin," *Appl. Opt.*, vol. 34, 1995, pp. 7410-7418.

[88] Y. Komai and T. Ushiki, "The three-dimensional organization of collagen fibrils in the human cornea and sclera," *Invest. Ophthal. Vis. Sci.*, vol. 32, 1991, pp. 2244-2258.

[89] J.L. Cox, R.A. Farrell, R.W. Hart, et al., "The transparency of the mammalian cornea," *J. Physiol.*, vol. 210, 1970, pp. 601-616.

[90] D.W. Leonard and K.M. Meek, "Refractive indices of the collagen fibrils and extrafibrillar material of the corneal stroma," *Biophys. J.*, vol. 72, 1997, pp. 1382-1387.

[91] J.S. Maier, S.A. Walker, S. Fantini, et al., "Possible correlation between blood glucose concentration and the reduced scattering coefficient of tissues in the near infrared," *Opt. Lett.*, vol. 19, 1994, pp. 2062-2064.

[92] M. Kohl, M. Esseupreis, and M. Cope, "The influence of glucose concentration upon the transport of light in tissue-simulating phantoms," *Phys. Med. Biol.*, vol. 40, 1995, pp. 1267-1287.

[93] I.S. Grigoriev and E.Z. Meylikhov (eds.), *Physical Values: Handbook*, Moscow: Energoatomizdat, 1991.

[94] L. Wang, S.L. Jacques, and L. Zheng, "MCML – Monte Carlo modeling of light transport in multi-layered tissues," *Comp. Meth. Progr. Biomed.*, vol. 47, 1995, pp. 131-146.

[95] T.J. Farrell, M.S. Patterson, and B.C. Wilson, "A diffusion theory model of spatially resolved, steady-state diffuse reflectance for the noninvasive determination of tissue optical properties *in vivo*," *Med. Phys.*, vol. 19, 1992, pp. 879-88.

[96] J.G. Fujimoto and M.E. Brezinski, "Optical coherence tomography imaging," in *Biomedical Photonics Handbook*, ed. T. Vo-Dinh, Chap. 13, CRC Press, Boca Raton, FL, 2003.

[97] K.V. Larin, M. Motamedi, T.V. Ashitkov, et al., "Specificity of noninvasive blood glucose sensing using optical coherence tomography technique: a pilot study," *Phys. Med. Biol.*, vol. 48, 2003, pp. 1371-1390.

[98] R.O. Esenaliev, K.V. Larin, I.V. Larina, et al., "Noninvasive monitoring of glucose concentration with optical coherence tomography," *Opt. Lett.*, vol. 26, 2001, pp. 992-994.

[99] K.V. Larin, T. Akkin, R.O. Esenaliev, et al., "Phase-sensitive optical low-coherence reflectometry for the detection of analyte concentrations," *Appl. Opt.*, vol. 43, 2004, pp. 3408-3414.